Analyst

PAPER

View Article Online
View Journal | View Issue

Cite this: *Analyst*, 2025, **150**, 3147

Utilising highly conductive TPU "sticks" for facile and low-cost electroanalysis†

Ana C. M. Oliveira,[a,b] Elena Bernalte,[a] Robert D. Crapnell,[a] Rodrigo A. A. Muñoz[b] and Craig E. Banks*[a]

Rapid, on-site analysis of environmental contaminants necessitates the use of cost-effective and straightforward apparatus to encourage widespread adoption and align with the United Nations Sustainable Development Goal 6: Clean Water and Sanitation. In this work, we report the development of highly conductive thermoplastic polyurethane (TPU) filaments that can be easily cut and assembled into "sticks", functioning as standalone rod-like working electrodes for electrochemical and electroanalytical applications. Using TPU as the base polymer, filaments filled with 35, 40, and 45 wt% carbon black (CB) were fabricated and characterised both physicochemically and electrochemically at different lengths (2.5, 5 and 10 mm). Among these, the 45 wt% CB filaments demonstrated the best electrode performance. Interestingly, due to morphological differences between the cross-section and the outer surface of the filament, extending the length of the filament sticks to 10 mm resulted in significant splitting of electrochemical peaks. Consequently, 5 mm sticks were optimised and employed for the electroanalytical detection of acetaminophen, achieving a linear detection range of 5–800 μM, a detection limit of 1.74 μM, and a quantification limit of 5.70 μM. These sticks were further validated by successfully detecting acetaminophen in tap and river water samples. This work introduces an innovative approach to reducing costs and simplifying on-site electrochemical analysis by using predefined lengths of conductive plastic filaments, which can be conveniently transported and stored on a spool until needed. The simplicity and affordability of this method enhance the commercial viability of electroanalytical sensing technologies.

Received 28th April 2025,
Accepted 5th June 2025

DOI: 10.1039/d5an00472a

rsc.li/analyst

1 Introduction

In 2022, the United Nations (UNs) reported that 2.2 billion people lacked safely managed drinking water around the world. This is particularly addressed in the United Nations Sustainable Development Goal number 6 "Clean Water and Sanitation", which aims to ensure availability and sustainable management of water and sanitation for all.[1] Therefore, the monitoring of environmental contaminants acquires special relevance for the future of human health, biodiversity, and our planet. To achieve this, the waters must be regularly tested for potential pollutants to identify problematic areas. Current water quality assessment methods utilise large and expensive laboratory equipment, such as chromatographic techniques combined with mass spectrometry.[2] While these methods are well understood, reliable and accurate, they require skilled users, are expensive, and involve sample transportation and storage, and significant sample pretreatment. To improve the system for testing environmental waters, an on-site, portable, simple, and low-cost method to screen areas for potential risk would be greatly beneficial.[3] This would allow for specific samples of interest to be sent to laboratories for verification, greatly improving both the time and cost effectiveness of the process. Electroanalysis offers a potential solution to fill this technological gap due to its ease of use, rapid results, and affordable approach, especially with portable potentiostats readily available on the market.[4]

One growing area of electrochemical research is additive manufacturing electrochemistry, in particular the use of Fused Filament Fabrication (FFF). This functions through a layer-by-layer deposition of electrically conductive thermoplastic to create a final 3D object. The rise in popularity of additive manufacturing electrochemistry began due to the commercial availability of electrically conductive filament, which allowed the fabrication of 3D printed electrodes that have been applied for the determination of environmental contaminants, such as pesticides,[5] pharmaceuticals,[6–8] and heavy metals.[9,10] Although interesting, these systems generally do not compare

[a]*Faculty of Science and Engineering, Manchester Metropolitan University, Dalton Building, Chester Street, M1 5GD, Great Britain. E-mail: c.banks@mmu.ac.uk; Tel: +44(0)1612471196*
[b]*Institute of Chemistry, Federal University of Uberlândia, 38400-902 Uberlândia, Minas Gerais, Brazil*

† Electronic supplementary information (ESI) available. See DOI: https://doi.org/10.1039/d5an00472a

favourably with the use of other working electrodes due to the inherent poor conductivity of the filament used. Although researchers have rigorously tried to improve the performance of electrodes printed from this material through optimising the designs[11–13] and printing parameters,[14–16] or through "activating" the printed surface,[17–21] the performance of the resultant electrodes is still substandard for real applications.

Different approaches have been explored where researchers have focused on creating their own bespoke filament, which allows them to tailor their properties through changing the polymer, plasticiser, conductive filler compositions and loadings.[22] With poly(lactic acid) (PLA), the most explored base polymer for producing bespoke filament due to its natural synergy and familiarity within FFF additive manufacturing.[14,23–29] The focus started on increasing the conductive loadings within the filament,[30,31] followed by varying the carbon morphologies used aiming to create either enhanced conductive networks through the insulating polymer,[32,33] or to minimise the material cost for production.[34,35] Later, there has also been work on improving the sustainability of these filaments, aligning this field with the UNs Sustainable Development Goal 12 "Responsible Use and Consumption", whereby a move toward bio-based plasticisers[36–38] and the use of recycled PLA was tackled to promote novel conceptualisation on circular economy electrochemistry.[39,40] Although excellent improvements, these systems will always inherently be single use items due to the significant issue PLA has with water/solution ingress[41] and its poor chemical stability.[42]

To find alternative solutions to this, conductive filaments from different base polymers have been subsequently explored in the literature,[43] including poly(ethylene terephthalate glycol) (PETg)[44,45] and, more recently, poly(propylene) (PP),[46] which showed the anticipated improvement in the chemical properties of the conductive filaments while maintaining competitive electrochemical performance. Another possible base polymer identified for additive manufacturing electrochemistry is thermoplastic poly(urethane) (TPU), which adds interesting new features to the filaments because it is a flexible, durable, and resistant material. Due to its composition of alternative soft and hard blocks, it is resistant to abrasion, oils, and chemicals. There is a commercially available TPU although this has severely limited conductivity. As such, some researchers have looked to improve this by drop-casting carbon black onto its surface post-print, improving its performance somewhat.[47] More recently, bespoke filament has been made using carbon black or a combination of diamond and carbon nanotubes.[48,49] However, the main drawback of printing with TPU is that, as a softer material, it is known to be more difficult than standard materials such as PLA. This is highlighted in the two bespoke filament reports, which both had to utilise specially modified printers to enable adequate printing. Thus, its use for the production of electrodes would initially require skilled users/developers as well as specifically equipped 3D printing machines adapted to allow reliable printing of such soft materials.

Therefore, to encourage commercial uptake and address the initial challenges associated with flexible conductive TPU, we propose the use of simple sticks of filament as working electrodes, eliminating the need for additive manufacturing. This approach reduces both time and overall costs, as electrodes can be easily produced by measuring the desired length and cutting the filament directly from the spool. Given the cost-effectiveness of filament production and the simplicity of the methodology, we foresee it provides a practical solution to facilitate the commercial adoption of this new material.

2 Experimental section

2.1 Chemicals

All chemicals used throughout this work were used as received without any further purification. All aqueous solutions were prepared with deionised water of a measured resistivity not less than 18.2 MΩ cm, sourced from a Milli-Q Integral 3 system from Millipore UK (Watford, UK). Hexaammineruthenium(III) chloride (98%), potassium ferricyanide (99%), potassium ferrocyanide (98.5–102%), sodium hydroxide (>98%), acetaminophen (≥99%), potassium chloride (99.0–100.5%), and phosphate-buffered saline (PBS) tablets were purchased from Merck (Gillingham, UK). Carbon black (CB) was purchased from PI-KEM (Tamworth, UK). Thermoplastic poly(urethane) (TPU, Desmopan 3855) was purchased from Hardie Polymers (Glasgow, UK). Commercial conductive filaments from TPU (Ninjatek Eel) was purchased from 3D FilaPrint (Rochford, UK) and from PLA (Protopasta) purchased from Farnell (Leeds, UK).

2.2 Filament production

All TPU was dried in an oven at 60 °C for a minimum of 2.5 h before use to remove any residual water in the polymer. The polymer compositions were prepared through the addition of appropriate amounts of TPU and CB in a chamber of 63 cm^3. The compounds were mixed using a Thermo Haake Polydrive dynameter fitted with a Thermo Haake Rheomix 600 (Thermo-Haake, Germany) at 210 °C with Banbury rotors at 70 rpm for 5 min. The resulting polymer composites were allowed to cool to room temperature before being granulated to create a finer particle size using a Rapid Granulator 1528 (Rapid, Sweden). The polymer composites were collected and processed through the hopper of a EX2 extrusion line (Filabot, VA, United States). The EX2 was set up with a single screw with two set heat zones of 60 and 210 °C, respectively. The molten polymer was extruded from a 1.75 mm die head, pulled along an Airpath cooling line (Filabot, VA, United States) and collected on a spool.

2.3 Physicochemical characterisation

X-ray Photoelectron Spectroscopy (XPS) data were acquired using an AXIS Supra (Kratos, UK), equipped with a monochromatic Al X-ray source (1486.6 eV) operating at 225 W and a hemispherical sector analyser. It was operated in fixed trans-

mission mode with a pass energy of 160 eV for survey spectra and 20 eV for region spectra with the collimator operating in slot mode for an analysis area of approximately 700 × 300 μm, the FWHM of the Ag 3d5/2 peak using a pass energy of 20 eV was 0.613 eV. The binding energy scale was calibrated by setting the graphitic sp^2 C 1s peak to 284.5 eV; this calibration is acknowledged to be flawed[50] but was nonetheless used in the absence of reasonable alternatives, and because only limited information was to be inferred from absolute peak positions.

Scanning Electron Microscopy (SEM) micrographs were obtained using a Crossbeam 350 Focussed Ion Beam – Scanning Electron Microscope (FIB-SEM) (Carl Zeiss Ltd, Cambridge, UK) fitted with a field emission electron gun. Secondary electron imaging was completed using a Secondary Electron Secondary Ion (SESI) detector. Samples were mounted on the aluminium SEM pin stubs (12 mm diameter, Agar Scientific, Essex, UK) using adhesive carbon tabs (12 mm diameter, Agar Scientific, Essex, UK) and coated with a 5 nm layer of Au/Pd metal using a Leica EM ACE200 coating system before imaging.

Thermogravimetric analysis (TGA) was performed using a Discovery Series SDT 650 controlled by Trios Software (TA Instruments, DA, USA). Samples were mounted in alumina pans (90 μL) and tested using a ramp profile (10 °C min^{-1}) from 0–800 °C under N_2 (100 mL min^{-1}).

2.5 Electrochemical experiments

All electrochemical experiments were performed in triplicate on an Autolab 100N potentiostat controlled by NOVA 2.1.7 (Utrecht, The Netherlands). Sticks of filament were used with different working electrode lengths (2.5, 5 and 10 mm) defined by the application of an insulating wrap made of heat shrink tube (Fig. S1†). All electrodes were ensured to have the same connection lengths,[12] and then used alongside an external commercial Ag|AgCl/KCl (3 M) reference electrode with a nichrome wire counter electrode. All solutions of $[Ru(NH_3)_6]^{3+}$ were purged of O_2 thoroughly using N_2 prior to any electrochemical experiments. Solutions of $[Fe(CN)_6]^{4-/3-}$ were prepared with both ferricyanide $[Fe(CN)_6]^{3-}$ and ferrocyanide $[Fe(CN)_6]^{4-}$, each at a concentration of 1 mM in 0.1 M KCl, following the same procedure without the need for further degassing. For the electrochemical characterisations, scan rate studies were conducted using $[Fe(CN)_6]^{4-/3-}$ and $[Ru(NH_3)_6]^{3+}$ electrochemical probes. From these, the electrochemical surface area of the working electrodes was estimated through cyclic voltammetry using the Randles–Ševčić equation, based on the I *vs.* $v^{1/2}$ plot.[51] The peak current values corresponding to the reduction peaks of $[Ru(NH_3)_6]^{3+}$ and the oxidation peaks of $[Fe(CN)_6]^{4-/3-}$ were used for this estimation. Additionally, the heterogeneous electron transfer rate constant (k^0) was determined using the Nicholson method with the collected CV data.[52] Briefly, this method relates the kinetic parameter to the peak-to-peak separation (ΔE_p) obtained from cyclic voltammetry. For this purpose, ΔE_p values were extracted from the cyclic voltammograms at each scan rate, and the kinetic parameter was determined from ΔE_p using Nicholson's empirical relationship. The heterogeneous electron transfer rate constant (k^0) was then calculated considering the following parameters: the diffusion coefficient, the number of electrons transferred, the scan rate, and the physical constants F (Faraday constant), R (universal gas constant), and T (temperature in Kelvin).

Electrochemical impedance spectroscopy (EIS) was recorded in the frequency range 0.1 Hz to 100 kHz applying 10 mV of signal amplitude to perturb the system under quiescent conditions. NOVA 2.1.7 software was used to fit Nyquist plots obtained to adequate equivalent circuit.

Activation of the electrodes was performed before all electrochemical experiments. This was achieved electrochemically in NaOH (0.5 M), as described in the literature.[53] Briefly, the additive manufactured electrodes were connected as the working electrode, in conjunction with a nichrome wire coil counter and Ag|AgCl/KCl (3 M) reference electrode and placed in a solution of 0.5 M NaOH. Chronoamperometry was used to activate the additive manufactured electrodes by applying a set voltage of +1.4 V for 200 s, followed by applying −1.0 V for 200 s. The electrodes were then thoroughly rinsed with deionised water and dried under compressed air before further use. Acetaminophen (or paracetamol) quantification was carried out using differential pulse voltammetry (DPV) with a 0.01 mol L^{-1} PBS buffer solution as the supporting electrolyte. The voltammetric parameters applied were 50 ms for modulation time, 25 mV for modulation amplitude, and 5 mV for step potential. Baseline correction was performed to present the voltammograms.

For the analysis of acetaminophen in tap and river water samples, no-pretreatment of the real samples was performed. Only 20-fold and 50-fold dilutions with 0.01 M PBS were carried out for tap and river water, respectively. Then, tap water sample was spiked with 167 μmol L^{-1} of acetaminophen, while the river water sample was spiked with 200 μmol L^{-1} for subsequent addition and recovery studies.

3 Results and discussion

3.1 Production of CB/TPU filament and physicochemical characterisation

The production of bespoke conductive TPU filaments with 35 wt%, 40 wt%, and 45 wt% carbon black (CB) were prepared, as presented in Fig. 1A. Briefly, the appropriate amounts of CB and TPU were added to the chamber of a rheomixer set to 210 °C and mixed for 5 min. The resultant composite was first shredded and then passed through a single screw extruder, also set to 210 °C, to produce the final 1.75 mm filament. All three filaments produced showed excellent low-temperature flexibility, as seen within Fig. 1B, meaning that the excellent flexible properties associated with TPU are not lost in the addition of such high-loadings of CB. Note that no additional plasticiser was added into this filament. Although flexible, these filaments were difficult to reliably print on a standard commercial printer, hence why other reports have used custo-

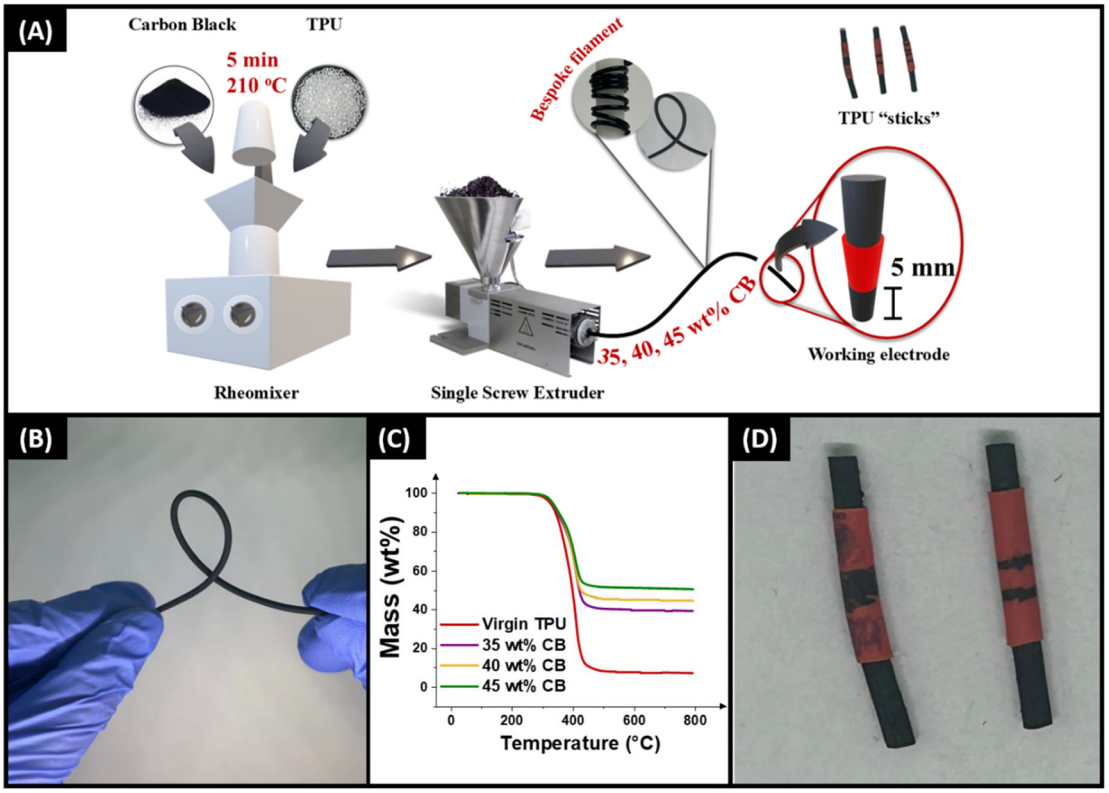

Fig. 1 (A) Schematic representation of filament production. (B) Photograph highlighting the low temperature flexibility of the 45 wt% CB/TPU filament. (C) Thermogravimetric analysis (TGA) of the virgin TPU and the 35, 40 and 45 wt% CB filaments. (D) Photographs of electrodes in the "stick" designs.

mised printers.[48,49] On testing, the 35 and 40 wt% filaments were able to be printed reliably on a customised printer, however for wider applicability we focus on the use of the filament as an electrode.

These filaments were analysed through thermogravimetric analysis (TGA), Fig. 1C, where crucial information about the effect that the inclusion of CB within TPU has on the thermal stability of the composite and the actual loadings of CB can be observed. Within Fig. 1C it can be observed that these loadings of CB within the TPU does not reduce the thermal stability of the polymer, with onset of degradation not decreasing. Following subtraction of the virgin TPU baseline, it was confirmed that the correct loadings of CB were indeed present within the filaments. Next, the resistivities of these filaments were tested the measurements of resistance across 10 cm, with values of 104.0 ± 7.8 Ω cm^{-1}, 30.9 ± 3.5 Ω cm^{-1}, and 14.7 ± 0.3 Ω cm^{-1} measured for the 35, 40 and 45 wt% CB/TPU filaments, respectively. These show the low resistivities that can be achieved using naturally flexible TPU polymeric matrix, without the addition of any plasticiser compound.

Within the literature, conductive filaments produced in the same way are then printed, using a FFF printer, into additive manufactured electrodes for electrochemical characterisation and electroanalytical applications.[22,32,35,36,45,46] This allows to utilise the advantages of additive manufacturing, such as the production of bespoke electrode geometries.[13] However, in this work, to maximise the efficiency of sensing platforms in regard to time, machinery, and cost, we remove this additional printing process. As such, we look to simply use the CB/TPU filament to perform the electrochemical and electroanalytical experiments. To achieve this, small "sticks" of filament were cut from the spool and wrapped in wire heat-shrink tubing to define the length of the exposed conductive filament, as seen in Fig. 1D. These sticks could then be treated in the same way as any other additive manufactured electrode, such as being "activated" to improve their electrochemical performance.

Electrochemical activation in NaOH (0.5 M) is a common strategy within additive manufacturing electrochemistry[53] to remove surface polymer and expose increase amounts of the graphitic carbon. Although commonly used for PLA based materials, this method has also been shown to improve the electrochemical activity of conductive PETg[44,45] and PP,[46] and as such, we look to use it for this conductive TPU. To understand how this procedure affects the physicochemical characteristics of the TPU sticks, they were subject initially to X-ray photoelectron spectroscopy (XPS). Fig. 2A and B present the survey spectrum and the C 1s spectrum, respectively, for the non-activated CB/TPU stick, with the same spectra shown for the activated sticks in Fig. 2C and D.

In both survey spectra, the expected peaks of oxygen, nitrogen, and carbon are present within TPU polymer. The main differences seen are the presence of silicon peaks, (Si 2p at

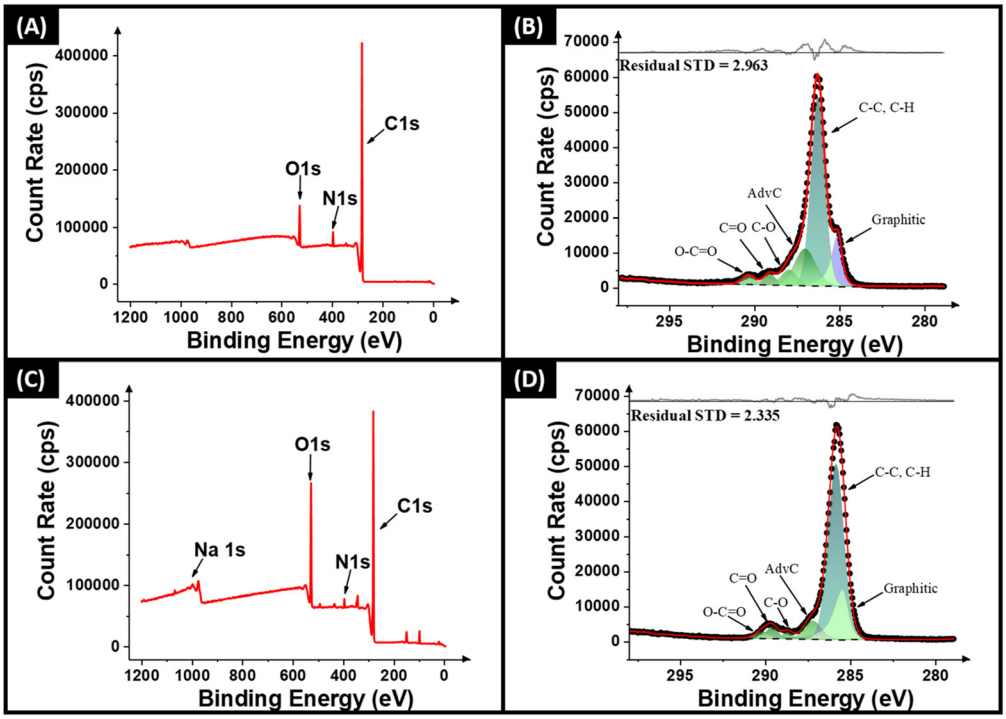

Fig. 2 XPS data of the 40 wt% CB/TPU filament: (A) Survey of non-activated filament; (B) C1s of non-activated filament; (C) Survey of activated filament; (D) C1s of activated filament.

~100 eV and Si 2s at ~150 eV), which can be due to the lubricants within the extrusion machinery, and the presence of a sodium peak, which is attributed to the NaOH solution used for activation. When looking at the C 1s spectra in Fig. 2B and D, similar characteristics can be seen where five symmetric peaks are required for adequate fitting, of which four are assigned to the expected sp^3 carbon binding environments of C–C, C–O, C═O, and O–C═O, respectively, as the binding energy increases. The additional symmetric peak detected is assigned to an adventitious carbon peak (Adv C), which is a thin layer of carbonaceous material commonly found on the surface of air exposed samples. The final peak, at the lowest binding energy, is an asymmetric peak attributed to the sp^2 carbon giving the X-ray photoelectron emission of graphitic carbon.[54,55] There is a significant change in the magnitude of the graphitic carbon peak between the non-activated and activated samples, growing from 13 wt% to 36 wt%, indicating that this process does reveal increased amounts of conductive filler. To confirm this, scanning electron microscopy (SEM) was performed on both the surface of the filaments and their cross-sections before and after activation.

Fig. 3A shows the surface of the non-activated 40 wt% TPU filament, with the cross-section seen in Fig. 3B. The corresponding images for the activated samples are seen in Fig. 3C and D. For the outer surface of the filament sticks, for the non-activated sample, there are some small spherical-shaped protrusions of carbon black on the surface, but a complete covering of polymer is observed. In comparison for the activated sample, while such covering of polymer is still visible, there is much larger undulations detected as well as significant perforations. These indicate enhanced surface conductive carbon, and that solution may be able to access conductive filler deeper into the filament structure further aiding the electrochemical performance. When comparing the cross-section SEMs, the structures observed are very similar, Fig. 3B and D. In both cases, small nanometre spherical particles of carbon black can be seen alongside the characteristic stretched polymeric structure of TPU, which originates from the combination of soft and hard blocks in its chemical structure. Due to the increase in graphitic carbon seen within the XPS and SEM, all samples were activated prior to electrochemical use.

3.2 Electrochemical characterisation of filament sticks

Once physicochemically characterised, the electrochemical performance of the conductive TPU sticks was explored. Fig. S2† shows the cyclic voltammograms (scan rate 100 mV s^{-1}) obtained for the bespoke 45 wt% CB filament (red) and the commercial conductive TPU (black) against $[Ru(NH_3)_6]^{3+}$ (1 mM in 0.1 M KCl). Note that the length of the electrode used for these analyses was 5 mm. In a first inspection for the bespoke 45 wt% CB/TPU filament, it is confirmed the presence of well-defined reduction and oxidation peaks, whereas no redox process is visible using the same length of electrode fabricated using the commercial filament. This highlights the potential of these bespoke filaments compared to existing options. As such, the bespoke filaments were tested through

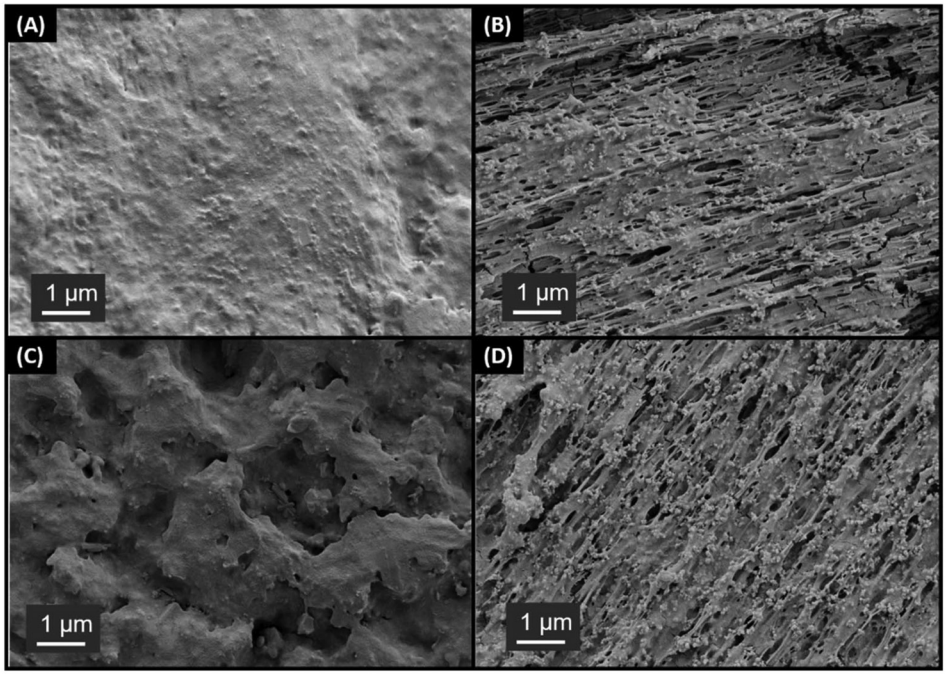

Fig. 3 SEM images of the 40 wt% CB/TPU filaments: (A) External surface non-activated; (B) cross section non-activated; (C) external surface activated; (D) cross section activated.

cyclic voltammograms scan rate studies, firstly against the near-ideal outer-sphere redox probe $[Ru(NH_3)_6]^{3+}$ (1 mM in 0.1 M KCl), which allows the most accurate determination of the heterogeneous electron (charge) transfer rate constant (k^0) and the real electrochemical surface area (A_e).[51,56]

An example of the scan rate study (5–500 mV s^{-1}) obtained for the bespoke filament 40 wt% CB/TPU filament is shown in Fig. 4A, with the 35 and 45 wt% shown in Fig. S3,† with their associated Randles–Ševčík plot inset. A clear, well-defined reduction peak is seen with minimal cathodic shift indicating an excellent performance; however there is less definition in the associated oxidation peak. This is less pronounced when observing the results against the commonly used inner-sphere redox probe $[Fe(CN)_6]^{4-}$ (1 mM in 0.1 M KCl), Fig. 4B and S3.† In this case, there are well-defined oxidation and reduction peaks, with a linear inset Randles–Ševčík plot showing the diffusion-controlled nature of the process. The key electrochemical results obtained from these studies are presented in Table 1. These include the heterogeneous electron transfer rate constant (k^0), which reflects the ease of electron transfer, the peak-to-peak separation (ΔE_p), which provides insight into the reversibility of the redox process, the electroactive surface area, as well as the charge transfer resistance (R_{ct}) and solution resistance (R_s).

Fig. 4C shows a comparison of the cyclic voltammograms (100 mV s^{-1}) obtained for the three different "stick" electrodes produced from the 40 wt% CB/TPU filament against $[Fe(CN)_6]^{4-}$ (1 mM in 0.1 M KCl). This shows adequate reproducibility between different electrodes considering that they are produced simply by cutting a piece of filament. According to the Table 1, slightly higher values of k^0 and lower ΔE_p were obtained for the electrodes fabricated using the filaments containing 40 wt% carbon black. This may be associated with a more homogeneous and reliable filament structure, ultimately enhancing the overall electrochemical performance of the electrode. However, when the standard deviations are taken into account, no statistically significant differences are observed among the three compositions. This indicates that the filament composition, within the range studied, does not substantially affect these electrochemical parameters. The filaments were then tested through electrochemical impedance spectroscopy (EIS) with the Nyquist plots shown in Fig. 4D and E. Within Fig. 4D, the commercially available conductive TPU filament is included showing the significantly larger charge-transfer resistance (R_{CT}). Fig. 4E removes the commercial filament to allow further scrutiny of the bespoke CB/TPU filaments made within this work. From this and Table 1, it can be seen that the R_S for the 35 wt% CB/TPU filament produces the highest resistance as expected, but interestingly, the 40 wt% filament gave a slightly lower value than the 45 wt%. When considering the R_{CT}, however, the expected trend is seen with the 35 wt% filament producing a value of 12.2 ± 1.4 kΩ, compared to 6.6 ± 1.4 kΩ for the 40 wt%, and 4.8 ± 0.6 kΩ for the 45 wt% filament. This clearly indicates that the best performance comes from the 45 wt% CB/TPU filament.

3.3 Study of the length influence on the electrochemical performance of the sticks

Based on the electrochemical results and the SEM images reported in this work, it is interesting to evaluate the effect of

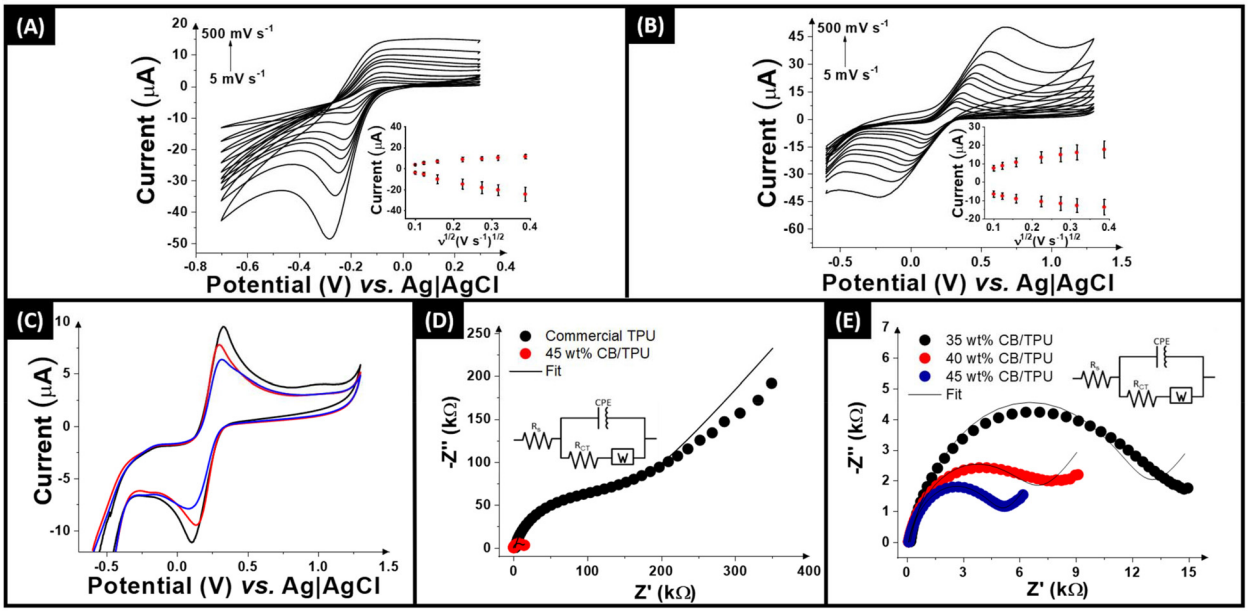

Fig. 4 Cyclic voltammogram scan rate study (5–500 mV s^{-1}) with (A) $[Ru(NH_3)_6]^{3+}$ (1 mM in 0.1 M KCl) and (B) $[Fe(CN)_6]^{4-}$ (1 mM in 0.1 M KCl) performed in the 40 wt% CB/TPU filament. Inset: the Randles–Ševčík plot. (C) Cyclic voltammograms (100 mV s^{-1}) of three 40 wt% CB/TPU electrodes (run separately) in the presence of $[Fe(CN)_6]^{4-}$ (1 mM in 0.1 M KCl) at the same conditions. EIS Nyquist plots of $[Fe(CN)_6]^{4-/3-}$ comparing (D) 45 wt% CB/TPU filament with commercial filament and (E) 35, 40 and 45 wt% CB/TPU filament. Inset: the proposed equivalent circuit.

Table 1 Summary of the electrochemical characteristics calculated through the scan rate studies and electrochemical impedance spectroscopy

	35 wt%	40 wt%	45 wt%
ΔE_p [a] (mV)	361 ± 138	157 ± 64	333 ± 132
k^0 [c] ($\times 10^{-3}$ cm s^{-1})	3.8 ± 0.1	4.5 ± 0.5	3.9 ± 0.2
A_e [c] (cm^2)	0.05 ± 0.01	0.05 ± 0.02	0.09 ± 0.02
ΔE_p [b] (mV)	445 ± 107	238 ± 58	323 ± 54
k^0 [d] ($\times 10^{-3}$ cm s^{-1})	3.4 ± 0.1	3.6 ± 0.2	3.4 ± 0.1
R_S [e] (Ω)	183.6 ± 1.2	93.3 ± 0.9	111.1 ± 0.4
R_{CT} [e] (kΩ)	12.2 ± 1.4	6.6 ± 1.4	4.8 ± 0.6

[a] Extracted from 25 mV s^{-1} cyclic voltammogram of $[Ru(NH_3)_6]^{3+}$ (1 mM in 0.1 M KCl). [b] Extracted from 25 mV s^{-1} cyclic voltammogram of $[Fe(CN)_6]^{4-}$ (1 mM in 0.1 M KCl). [c] Calculated using $[Ru(NH_3)_6]^{3+}$ cyclic voltammetric scan rate study performed between 5 and 500 mV s^{-1}. [d] Calculated using $[Fe(CN)_6]^{4-}$ cyclic voltammetric scan rate study performed between 5 and 500 mV s^{-1}. [e] Extracted from Nyquist plots of EIS experiments in $[Fe(CN)_6]^{4-/3-}$ (1 mM in 0.1 M KCl). All measurements were performed with a nichrome wire CE and Ag|AgCl (3 M KCl) RE. Errors reported in Table 1 refer to standard deviations of the measurements.

the filament length on the electrochemical performance of the TPU stick electrodes. From Fig. 3, a significant difference can be seen between the cross-section and surface of the filament. Each "stick" used within this work is comprised of both one cross-section and then the outer circumference. As such, increasing the area of the outer circumference was studied by using "sticks" of 2.5 mm, 5 mm and 10 mm as shown in Fig. S1.† The performance of these electrodes toward both the outer and inner-sphere probes studied above can be seen in Fig. 5, with the 2.5 mm results in A and D, 5 mm in B and E, and 10 mm in C and F.

Interestingly, within the cyclic voltammograms obtained against $[Ru(NH_3)_6]^{3+}$ (1 mM in 0.1 M KCl) the 2.5 mm electrode shows a more well-defined oxidation peak when compared to the 5 mm electrode. In contrast, the 10 mm electrode shows splitting of both the oxidation and reduction peaks, indicating a significant difference in the electron transfer properties of the electrode when the amount of outer surface circumference is increased. This phenomenon is not observed with the inner-sphere redox probe $[Fe(CN)_6]^{4-}$ (1 mM in 0.1 M KCl), although the electron transfer kinetics for this species is lower than its ruthenium counterpart. Due to the advantage of an increased electrochemical area in terms of the peak current, and the disruption to the electrochemical performance seen for the 10 mm electrode, the 5 mm electrode was chosen for use within the electroanalytical application.

3.4 Application to the detection of acetaminophen in environmental waters

To test how the filament "sticks" function as an electrode for an electroanalytical application, it was applied to the determination of acetaminophen (ACET). Acetaminophen was selected as a model analyte due to its widespread use as an over-the-counter analgesic and antipyretic, which has led to its frequent detection in environmental waters as a pharmaceutical contaminant. When consumed in excess, acetaminophen is excreted in urine, contributing to the contamination of water bodies and, consequently, drinking water supplies.[57] As a result, there is growing interest in developing analytical

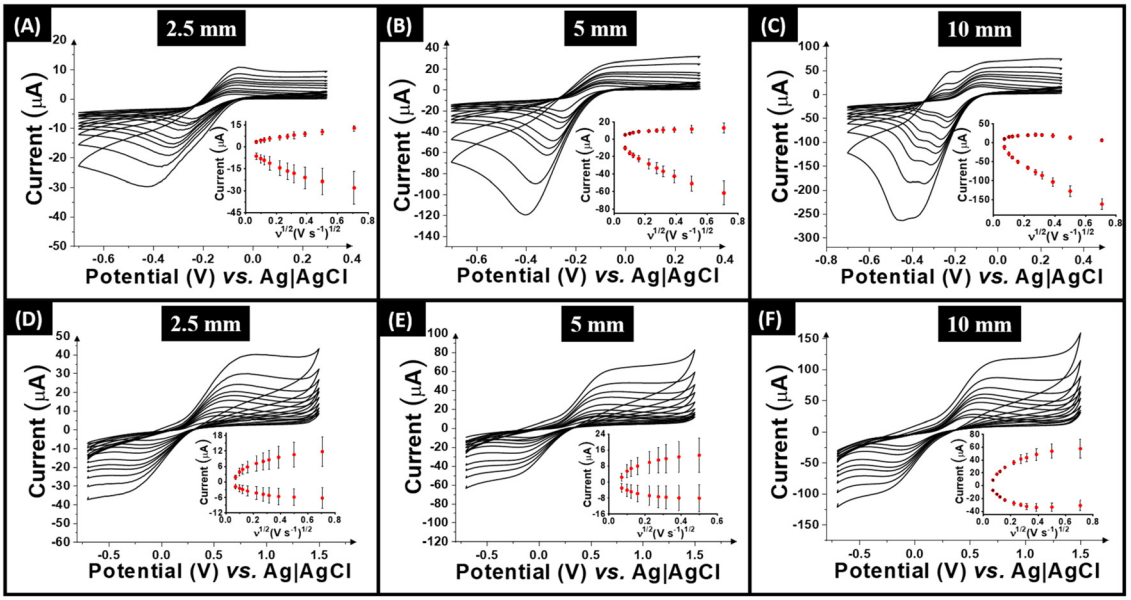

Fig. 5 Cyclic voltammogram scan rate study (5–500 mV s^{-1}) with $[Ru(NH_3)_6]^{3+}$ (1 mM in 0.1 M KCl) performed in the 40 wt% CB/TPU filaments with different sizes. Inset: the Randles–Ševčík plot: (A) 2.5 mm; (B) 5 mm; (C) 10 mm. Scan rate study (5–500 mV s^{-1}) with $[Fe(CN)_6]^{4-/3-}$ (1 mM in 0.1 M KCl) performed in the 40 wt% CB/TPU filaments with different sizes. Inset: the Randles–Ševčík plot: (D) 2.5 mm; (E) 5 mm; (F) 10 mm.

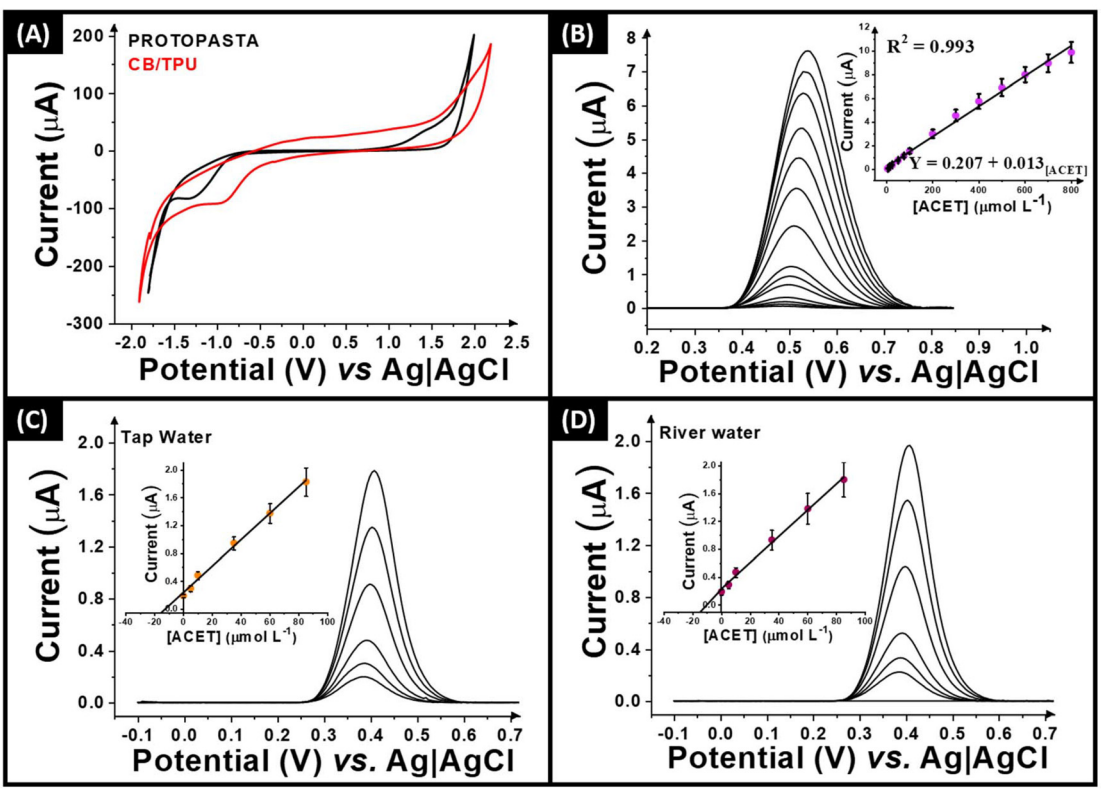

Fig. 6 (A) Cyclic voltammograms recorded in 0.1 mol L KCl to study the potential window using Protopasta and 45 wt% CB/TPU as working electrodes. Scan rate: 50 mV s^{-1}. (B) Differential pulse voltammograms of ACET in different concentrations in 0.01 M PBS (pH 7.5) recorded at 5 mm filament and the respective calibration curve inset. Differential pulse voltammograms of spiked (C) tap water sample diluted (20-fold) and (D) river water sample diluted (50-fold) in 0.01 M PBS pH 7.5 with subsequent additions of ACET standard solutions. Inset: standard calibration plots. Step potential: 5 mV. Amplitude: 25 mV.

methods for the quantification of this compound in water samples, since the presence of acetaminophen in aquatic environments can cause adverse ecological impacts and compromise drinking water safety. Currently, acetaminophen is typically detected using techniques such as high-performance liquid chromatography (HPLC), liquid chromatography-mass spectrometry (LC-MS) and spectrometry.[57] Although these methods provide high sensitivity and accuracy, they rely on expensive instrumentation and are not suitable for on-site or rapid analysis. While legal limits for acetaminophen in water are not universally defined, several studies in the literature report detection limits (LOD) in the micromolar (μmol L^{-1}) range for its determination in water.[57]

Firstly, the potential window of the filament was established within 0.1 M KCl, Fig. 6A, where it is compared to the commonly used commercially available conductive PLA (Protopasta) as the TPU gave no response. It can be seen that the 45 wt% CB/TPU was able to reach higher anodic potentials than the PLA and was more than enough for the detection of ACET.

Fig. 6B presents the differential pulse voltammograms of ACET within 0.01 M PBS (pH = 7.5) for additions between 5–800 μM, with the associated calibration plot inset. A linear curve of R^2 = 0.993 was achieved in this concentration range with the equation of the line equal to $y = 0.207 + 0.013_{[ACET]}$. Using this plot, the limit of detection (LOD) and limit of quantification (LOQ) were calculated using 3 and 10 times the standard deviation of the blank divided by the slope of the best fit as 1.74 μM and 5.70 μM, respectively. The excellent LOD and R^2 values obtained show how using simple, defined pieces of the filament were able to achieve excellent electroanalytical results. To further prove this, the "sticks" were used for the detection of ACET within real tap and river water samples, Fig. 6C and D. In both cases adequate recovery levels were found of 123% and 121%, respectively.

This work presents the fabrication of highly conductive TPU filament through incorporation of CB and its characterisation. Importantly, the filament is not used for additive manufacturing and instead removes this construction step and simply uses the cut filament at a defined length for electrochemical and electroanalytical experiments. This shows a unique strategy to lower the cost and further simplify the process of on-site analysis using electrochemistry.

4 Conclusions

In this work, we report the fabrication of conductive TPU filament through in incorporation of 35 wt%, 40 wt% and 45 wt% carbon black. The filaments were then physicochemically characterised through TGA, XPS, and SEM. Next, instead of utilising the filament for additive manufacturing, the filament itself of a defined length was utilised as a working electrode. Through electrochemical characterisation against both $[Ru(NH_3)_6]^{3+}$ and $[Fe(CN)_6]^{4-}$, it was found that the 45 wt% filament performed the best. Interestingly, it was found that increasing the length of filament "sticks" from 5 mm to 10 mm saw the splitting of the redox peaks of $[Ru(NH_3)_6]^{3+}$, which was attributed to the larger area of polymer covered outer filament in comparison to the porous and more graphitic carbon rich cross-section. The 5 mm filament sticks were then applied toward the detection of acetaminophen (ACET), where a linear range between 5–800 μM was obtained along with a LOD of 1.74 μM and LOQ of 5.70 μM. The "sticks" were then successfully used for the detection of ACET within tap and river water.

This work presents a unique strategy to lower the cost and further simplify the process of on-site analysis using electrochemistry by employing defined lengths of conductive plastic, which can be easily transported and stored on the spool before use. The simplicity and cost-effectiveness of this approach could enhance the commercial potential of electroanalytical sensing platforms. Furthermore, the attractive features of TPU, combined with its use as the polymer matrix in this study, contribute to and open opportunities for further exploration of this material for the development of sensors in various configurations and through alternative sources, such as the use of recycled polymers, thereby contributing to the advancement of a circular economy in electrochemistry.

Data availability

The data supporting this article have been included in the main paper and as part of the ESI.†

Conflicts of interest

The authors declare that they have no known competing financial interests or personal relationships that could have appeared to influence the work reported in this paper.

Acknowledgements

We thank Dr Hayley G. Andrews for obtaining the SEM micrographs and Bruno Ferreira for running the TGA samples. We would also like to thank the EPSRC (EP/W033224/1) and Horizon Europe (grant 101137990) for funding, CNPq (Conselho Nacional de Desenvolvimento Científico e Tecnológico) grants 140406/2021-2 and 401681/2023-8, and Coordenação de Aperfeiçoamento de Pessoal de Nível Superior (CAPES) grant 88887.836030/2023-00.

References

1 U. Nations, United Nations Sustainable Development Goal number 6 "Clean Water and Sanitation", **https://sdgs.un.org/goals/goal6#overview**, (accessed 12/11/2024, 2024).
2 R. Sivaranjanee, P. S. Kumar, R. Saravanan and M. Govarthanan, *Chemosphere*, 2022, **294**, 133779.

3 J. Muñoz and M. Pumera, *ChemElectroChem*, 2020, **7**, 3404–3413.
4 M. Cuartero, *Sens. Actuators, B*, 2021, **334**, 129635.
5 B. C. Janegitz, R. D. Crapnell, P. Roberto de Oliveira, C. Kalinke, M. J. Whittingham, A. Garcia-Miranda Ferrari and C. E. Banks, *ACS Meas. Sci. Au*, 2023, **3**, 217–225.
6 R. D. Crapnell, E. Bernalte, A. G.-M. Ferrari, M. J. Whittingham, R. J. Williams, N. J. Hurst and C. E. Banks, *ACS Meas. Sci. Au*, 2021, **2**, 167–176.
7 M. Di-Oliveira, D. A. Araújo, D. L. Ramos, L. V. de Faria, R. G. Rocha, R. M. Sousa, E. M. Richter, T. R. Paixão and R. A. Munoz, *Electrochim. Acta*, 2024, **481**, 143945.
8 T. P. Lisboa, G. F. Alves, L. V. de Faria, C. C. de Souza, M. A. C. Matos and R. C. Matos, *Talanta*, 2022, **247**, 123610.
9 D. P. Rocha, A. L. Squissato, S. M. da Silva, E. M. Richter and R. A. Munoz, *Electrochim. Acta*, 2020, **335**, 135688.
10 J. G. Walters, S. Ahmed, I. M. Terrero Rodríguez and G. D. O'Neil, *Electroanalysis*, 2020, **32**, 859–866.
11 E. Bernalte, R. D. Crapnell, O. M. Messai and C. E. Banks, *ChemElectroChem*, 2024, e202300576.
12 R. D. Crapnell, A. Garcia-Miranda Ferrari, M. J. Whittingham, E. Sigley, N. J. Hurst, E. M. Keefe and C. E. Banks, *Sensors*, 2022, **22**, 9521.
13 A. G.-M. Ferrari, N. J. Hurst, E. Bernalte, R. D. Crapnell, M. J. Whittingham, D. A. Brownson and C. E. Banks, *Analyst*, 2022, **147**, 5121–5129.
14 C. Iffelsberger, C. W. Jellett and M. Pumera, *Small*, 2021, **17**, 2101233.
15 R. S. Shergill, C. L. Miller and B. A. Patel, *Sci. Rep.*, 2023, **13**, 339.
16 R. S. Shergill and B. A. Patel, *ChemElectroChem*, 2022, **9**, e202200831.
17 C. Kalinke, N. V. Neumsteir, G. de Oliveira Aparecido, T. V. de Barros Ferraz, P. L. Dos Santos, B. C. Janegitz and J. A. Bonacin, *Analyst*, 2020, **145**, 1207–1218.
18 D. P. Rocha, R. G. Rocha, S. V. Castro, M. A. Trindade, R. A. Munoz, E. M. Richter and L. Angnes, *Electrochem. Sci. Adv.*, 2022, **2**, e2100136.
19 R. S. Shergill and B. A. Patel, *ACS Appl. Electron. Mater.*, 2023, **5**, 5120–5128.
20 R. S. Shergill, F. Perez, A. Abdalla and B. A. Patel, *J. Electroanal. Chem.*, 2022, **905**, 115994.
21 R. J. Williams, R. D. Crapnell, T. Brine and C. E. Banks, *Electroanalysis*, 2024, **36**, e202400075.
22 R. D. Crapnell, C. Kalinke, L. R. G. Silva, J. S. Stefano, R. J. Williams, R. A. A. Munoz, J. A. Bonacin, B. C. Janegitz and C. E. Banks, *Mater. Today*, 2023, **71**, 73–90.
23 P. F. Flowers, C. Reyes, S. Ye, M. J. Kim and B. J. Wiley, *Addit. Manuf.*, 2017, **18**, 156–163.
24 K. Ghosh, S. Ng, C. Iffelsberger and M. Pumera, *Appl. Mater. Today*, 2022, **26**, 101301.
25 K. Ghosh, S. Ng, C. Iffelsberger and M. Pumera, *Chem. – Eur. J.*, 2020, **26**, 15746–15753.
26 S. L. Marasso, M. Cocuzza, V. Bertana, F. Perrucci, A. Tommasi, S. Ferrero, L. Scaltrito and C. F. Pirri, *Rapid Prototyping J.*, 2018, **24**, 739–743.
27 S. Nouseen, K. Ghosh and M. Pumera, *Electrochem. Commun.*, 2024, **160**, 107652.
28 J. S. Stefano, L. R. G. e. Silva, R. G. Rocha, L. C. Brazaca, E. M. Richter, R. A. A. Muñoz and B. C. Janegitz, *Anal. Chim. Acta*, 2022, **1191**, 339372.
29 J. S. Stefano, L. R. G. e. Silva and B. C. Janegitz, *Microchim. Acta*, 2022, **189**, 414.
30 I. V. Arantes, R. D. Crapnell, M. J. Whittingham, E. Sigley, T. R. Paixão and C. E. Banks, *ACS Appl. Eng. Mater.*, 2023, **1**, 2397–2406.
31 P. Wuamprakhon, R. D. Crapnell, E. Sigley, N. J. Hurst, R. J. Williams, M. Sawangphruk, E. M. Keefe and C. E. Banks, *Adv. Sustainable Syst.*, 2023, **7**, 2200407.
32 R. D. Crapnell, I. V. Arantes, J. R. Camargo, E. Bernalte, M. J. Whittingham, B. C. Janegitz, T. R. Paixão and C. E. Banks, *Microchim. Acta*, 2024, **191**, 96.
33 R. D. Crapnell, I. V. Arantes, M. J. Whittingham, E. Sigley, C. Kalinke, B. C. Janegitz, J. A. Bonacin, T. R. Paixão and C. E. Banks, *Green Chem.*, 2023, **25**, 5591–5600.
34 I. V. Arantes, R. D. Crapnell, E. Bernalte, M. J. Whittingham, T. R. Paixão and C. E. Banks, *Anal. Chem.*, 2023, **95**, 15086–15093.
35 K. K. Augusto, R. D. Crapnell, E. Bernalte, S. Zighed, A. Ehamparanathan, J. L. Pimlott, H. G. Andrews, M. J. Whittingham, S. J. Rowley-Neale and O. Fatibello-Filho, *Microchim. Acta*, 2024, **191**, 375.
36 R. D. Crapnell, I. V. Arantes, M. J. Whittingham, E. Sigley, C. Kalinke, B. C. Janegitz, J. A. Bonacin, T. R. Paixão and C. E. Banks, *Green Chem.*, 2023, **25**, 5591–5600.
37 J. P. C. Silva, R. G. Rocha, G. P. Siqueira, C. F. Nascimento, M. H. Santana, E. Nossol, E. M. Richter, I. S. da Silva and R. A. Muñoz, *Microchim. Acta*, 2025, **192**, 1–12.
38 L. R. Silva, L. V. Bertolim, J. S. Stefano, J. A. Bonacin, E. M. Richter, R. A. Munoz and B. C. Janegitz, *Electrochim. Acta*, 2025, **513**, 145566.
39 R. D. Crapnell, E. Sigley, R. J. Williams, T. Brine, A. Garcia-Miranda Ferrari, C. Kalinke, B. C. Janegitz, J. A. Bonacin and C. E. Banks, *ACS Sustainable Chem. Eng.*, 2023, **11**, 9183–9193.
40 E. Sigley, C. Kalinke, R. D. Crapnell, M. J. Whittingham, R. J. Williams, E. M. Keefe, B. C. Janegitz, J. A. Bonacin and C. E. Banks, *ACS Sustainable Chem. Eng.*, 2023, **11**, 2978–2988.
41 R. J. Williams, T. Brine, R. D. Crapnell, A. G.-M. Ferrari and C. E. Banks, *Mater. Adv.*, 2022, **3**, 7632–7639.
42 K. S. Erokhin, E. G. Gordeev and V. P. Ananikov, *Sci. Rep.*, 2019, **9**, 20177.
43 L. Xing and A. J. Casson, *Sens. Actuators, A*, 2023, **349**, 114062.
44 J. R. Camargo, R. D. Crapnell, E. Bernalte, A. J. Cunliffe, J. Redfern, B. C. Janegitz and C. E. Banks, *Appl. Mater. Today*, 2024, **39**, 102285.
45 R. D. Crapnell, E. Bernalte, E. Sigley and C. E. Banks, *RSC Adv.*, 2024, **14**, 8108–8115.
46 D. L. Ramos, R. D. Crapnell, R. Asra, E. Bernalte, A. Oliveira, R. A. Muñoz, E. M. Richter, A. M. Jones and

C. E. Banks, *ACS Appl. Mater. Interfaces*, 2024, **16**, 56006–56018.
47 L. Gullo, V. Mazzaracchio, N. Colozza, L. Duranti, L. Fiore and F. Arduini, *Electrochim. Acta*, 2024, **482**, 143982.
48 S. Baluchová, S. van Leeuwen, B. Kumru and J. G. Buijnsters, *ACS Appl. Polym. Mater.*, 2024, **6**, 14638–14647.
49 A. C. Oliveira, E. Bernalte, R. D. Crapnell, M. J. Whittingham, R. A. Munoz and C. E. Banks, *Appl. Mater. Today*, 2025, **42**, 102597.
50 G. Greczynski and L. Hultman, *Sci. Rep.*, 2021, **11**, 1–5.
51 A. García-Miranda Ferrari, C. W. Foster, P. J. Kelly, D. A. Brownson and C. E. Banks, *Biosensors*, 2018, **8**, 53.
52 R. S. Nicholson, *Anal. Chem.*, 1965, **37**, 1351–1355.
53 E. M. Richter, D. P. Rocha, R. M. Cardoso, E. M. Keefe, C. W. Foster, R. A. Munoz and C. E. Banks, *Anal. Chem.*, 2019, **91**, 12844–12851.
54 R. Blume, D. Rosenthal, J. P. Tessonnier, H. Li, A. Knop-Gericke and R. Schlögl, *ChemCatChem*, 2015, **7**, 2871–2881.
55 T. R. Gengenbach, G. H. Major, M. R. Linford and C. D. Easton, *J. Vac. Sci. Technol., A*, 2021, **39**, 013204.
56 R. D. Crapnell and C. E. Banks, *Talanta Open*, 2021, **4**, 100065.
57 L. M. A. Melo, K. A. O. Souza, J. E. B. Lopes, R. A. A. Muñoz, J. L. Costa and W. T. P. dos Santos, *Anal. Chim. Acta*, 2025, **1333**, 343243.